

Kinematic Displacement Analysis of a Double-Cardan-Joint Driveline

I. S. Fischer

Assistant Professor.
Mem. ASME

New Jersey Institute of Technology,
Newark, NJ 07102

R. N. Paul

Mem. ASME
W. R. Grace & Co.,
Columbia, MD 21044

The input-output displacement relations of two Cardan joints arranged in series on a driveline has been investigated in detail, including the effects of unequal joint angles, the phase angle between the two Cardan joints and also such manufacturing tolerance errors as nonright angle moving link lengths and offset joint axes. A combined Newton-Raphson method and Davidon-Fletcher-Powell optimization algorithm using dual-number coordinate-transformation matrices was employed to perform the analysis. An experiment was conducted to validate the results of the analysis. The apparatus consisted of a double-Cardan-joint driveline whose rotations were measured by optical shaft encoders that were sampled by a computer data-acquisition system. The equipment was arranged so that the phase angle between the joints and the offset angles between the shafts at each of the two joints could be readily varied. The "relative phase angle," the difference between the phase angle of the two joints and the angle between the planes defined by the input and intermediate and the intermediate and output shafts, was found to be the significant factor. If the offset angles at both Cardan joints are equal, the double-Cardan-joint driveline functions as a constant-velocity coupling when the magnitude of the relative phase angle is zero. If the offset angles at the two Cardan joints are unequal, a condition prevailing in the important front-wheel-drive automobile steering-column application, then fluctuation in output velocity for a constant input velocity is minimized although not eliminated for zero relative phase angle.

Introduction

The double-Cardan-joint driveline has been extensively used as a driveline in machinery, particularly the Hotchkiss automotive drive. The geometry of an application is specified by the offset angles (the angle between the input and intermediate shafts at the driving Cardan joint and the angle between the intermediate and output shaft and the driven Cardan joint) and by the shaft offset (the minimum distance between the input and output shaft axes). In most applications the mechanism is arranged so that the offset angles at the two Cardan joints are equal and all the shafts are in the same plane. Under those conditions the double-Cardan-joint driveline will operate as a constant-velocity coupling. Analyses of this arrangement are given in Doughtie and James (1954), in Tyson (1954), and also by Austin, Denavit, and Hartenberg (1965) who added consideration of manufacturing tolerance effects. If the shafts are in different planes and the offset angles are equal, then the Cardan joints can be phased relative to one another to produce a constant velocity coupling. This case was discussed by Mabie and Ocvirk (1975) and by Wagner (1979).

Recently, the double-Cardan-joint driveline has been used as a steering shaft in front-wheel-drive automobiles. As reported in Cowles and Chiu (1984), this application does not allow equal offset angles. The yokes of the two Cardan joints on the intermediate shaft are located in different planes, a pro-

cedure called joint phasing, in order to best approach constant-velocity output. Saari (1954) approached this problem by combining the input-output displacements for two Cardan joints, Phillip (1960) used a spherical-trigonometry analysis, Maziotti (1964) developed a vector procedure and Cooney (1966) has given an expression but not its derivation.

This study has modeled the double-Cardan-joint driveline with dual-number coordinate-transformation matrices and has applied numerical techniques to create a procedure for evaluating the effects of joint phasing and manufacturing tolerance errors on the input-output displacement relationship.

In addition, an experiment was conducted to validate the results of the numerical analysis.

Analysis

The ideal double-Cardan-joint driveline is a six link spatial mechanism with revolute joints. Although the Grübler equation predicts zero degrees of freedom, the mechanism operates because of its special proportions. If those special proportions are lost because of manufacturing tolerance errors such as nonright angle moving link lengths and offset joint axes, then it is necessary to consider one joint, in this study selected to be the output joint, as cylindrical to accommodate the sliding that occurs. This sliding motion is similar to that exhibited by the single Cardan joint as described in Fischer and Freuden-

Contributed by the Mechanisms Committee for publication in the JOURNAL OF MECHANICAL DESIGN. Manuscript received September 1989.

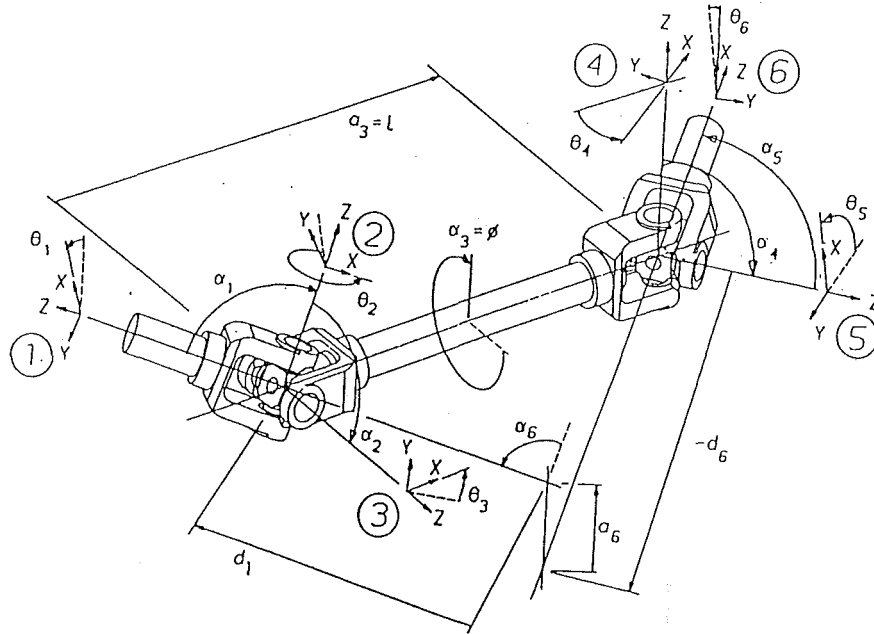


Fig. 1 Double-Cardan joint driveline

stein (1984). Therefore, this study will model the double-Cardan-joint driveline as an RRRRRC mechanism.

A double-Cardan-joint driveline is illustrated in Fig. 1. It has six joints numbered 1 through 6. At joint $i-1$ there is a coordinate frame fixed on the link connecting joints $i-1$ and i . Its position is specified by a z -axis aligned along the axis of joint $i-1$ and an x -axis aligned along the line of shortest distance between the axes of joints $i-1$ and i . The transformation between the coordinate frame on the link connecting joints $i-1$ and i and the coordinate frame on the link connecting joints i and $i+1$ can be expressed as a dual-number matrix

$$[\hat{A}_i] = \begin{bmatrix} c(\hat{\theta}_i) & -s(\hat{\theta}_i) & 0 \\ c(\hat{\alpha}_{i-1})s(\hat{\theta}_i) & c(\hat{\alpha}_{i-1})c(\hat{\theta}_i) & -s(\hat{\alpha}_{i-1}) \\ s(\hat{\alpha}_{i-1})s(\hat{\theta}_i) & s(\hat{\alpha}_{i-1})c(\hat{\theta}_i) & c(\hat{\alpha}_{i-1}) \end{bmatrix} \quad (1)$$

Equation (1) can be expanded into primary and dual components

$$[\hat{A}_i] = \begin{bmatrix} c(\theta_i) & -s(\theta_i) & 0 \\ c(\alpha_{i-1})s(\theta_i) & c(\alpha_{i-1})c(\theta_i) & -s(\alpha_{i-1}) \\ s(\alpha_{i-1})s(\theta_i) & s(\alpha_{i-1})c(\theta_i) & c(\alpha_{i-1}) \end{bmatrix} + \epsilon \begin{bmatrix} -d_i s(\theta_i) \\ d_i c(\alpha_{i-1})c(\theta_i) - a_{i-1} s(\alpha_{i-1})s(\theta_i) \\ d_i s(\alpha_{i-1})c(\theta_i) + a_{i-1} c(\alpha_{i-1})s(\theta_i) \\ -d_i c(\theta_i) & 0 \\ -d_i c(\alpha_{i-1})s(\theta_i) - a_{i-1} s(\alpha_{i-1})c(\theta_i) & -a_{i-1} c(\alpha_{i-1}) \\ -d_i s(\alpha_{i-1})s(\theta_i) + a_{i-1} c(\alpha_{i-1})c(\theta_i) & -a_{i-1} s(\alpha_{i-1}) \end{bmatrix} \quad (2)$$

The six links comprising the double-Cardan-joint driveline are connected serially to form a closed loop. This infers that the six transforms associated with the mechanism are related by the condition of loop closure:

$$[\hat{A}_1][\hat{A}_2] \dots [\hat{A}_6] = [\hat{I}] \quad (3)$$

where the dual-number identity matrix $[\hat{I}]$ is defined as

$$[\hat{I}] = \begin{bmatrix} 1 & 0 & 0 \\ 0 & 1 & 0 \\ 0 & 0 & 1 \end{bmatrix} + \epsilon \begin{bmatrix} 0 & 0 & 0 \\ 0 & 0 & 0 \\ 0 & 0 & 0 \end{bmatrix} \quad (4)$$

Equation (3) states that transforming from the frame fixed on one link in the mechanism through the frames fixed on each of the other links will result in a return to the original coordinate frame. This equation governs the kinematics of the double-Cardan-joint driveline.

The solution to the general form of equation (3) will be found by numerical methods. Duffy (1980) listed the solutions to various six-link mechanisms such as RCRRRR, RCRRRP, RRRCCR, and RRRCRP, but the displacement analysis of the RRRRRC by Ju and Duffy (1985) had not yet been published when it was decided to model the double-Cardan-joint driveline as an RRRRRC and obtain the displacements by a numerical scheme.

Dual-Number Formulation of Numerical Methods

The numerical methods used to determine the displacements of the double-Cardan-joint driveline are based on the algorithm introduced by Hall, Root, and Sandgren (1977) that combines the Davidon-Fletcher-Powell (DFP) optimization routine with the Newton-Raphson (NR) method as applied to kinematics by Uicker, Denavit, and Hartenberg (1964). These procedures were developed for use with 4×4 homogeneous transformation matrices, but for this study were adapted to 3×3 dual-number matrices.

The algorithm for the numerical solution is shown in flow-chart form in Fig. 2. The two methods of solution are available so that the most advantageous could be used depending upon the requirements at each position of the input variable. The DFP method is slower but will almost always find the displacements resulting in loop closure even if the initial guess of the displacements is poor, a condition that is troublesome for the NR method. If the initial guess of the displacements has been made reasonably well, the NR method is much faster. Thus the DFP method is used for the initial position of the input-link rotation when it is difficult to guess the displacements at the output and particularly the in-

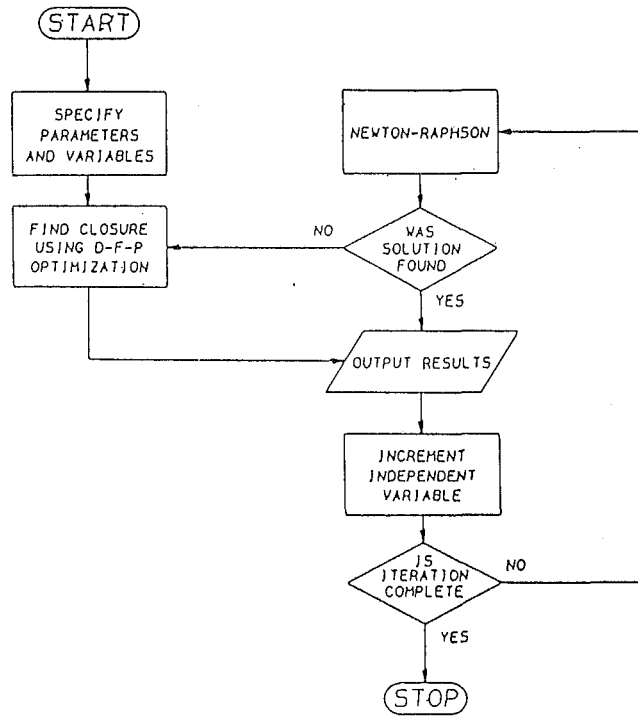


Fig. 2 Simplified flowchart of algorithm

intermediate joints. The NR method is used to determine the displacements associated with subsequent steps in the input-link rotation because if those steps are small, then the displacements determined for the previous input position are generally adequate as an initial guess. The displacements resulting in closure are usually found within a few iterations. Occasionally a solution cannot be found using the NR method and the algorithm will then use the DFP method to attempt to locate displacement values resulting in loop closure.

Details of the Newton-Raphson Method

A first-order expansion of equation (3) is

$$[\hat{A}_1][\hat{A}_2 + \hat{Q}_p \hat{A}_2 \delta \theta_2][\hat{A}_3 + \hat{Q}_r \hat{A}_3 \delta \theta_3] \\ [\hat{A}_4 + \hat{Q}_p \hat{A}_4 \delta \theta_4][\hat{A}_5 + \hat{Q}_r \hat{A}_5 \delta \theta_5][\hat{A}_6 + \hat{Q}_r \hat{A}_6 \delta \theta_6 + \\ \hat{Q}_p \hat{A}_6 \delta D_6] = \hat{I} \quad (5)$$

where \hat{A}_n are each evaluated at θ_n and D_n which are guesses of the displacement variables, $d\theta_n$ and dD_n are the errors between the guesses and exact values of the displacements, and \hat{Q}_r and \hat{Q}_p are the partial-derivative operators corresponding to equation (1) such that

$$[\hat{Q}_r] = \begin{bmatrix} 0 & -c(\alpha) + \epsilon as(\alpha) & -s(\alpha) - \epsilon ac(\alpha) \\ c(\alpha) - \epsilon as(\alpha) & 0 & 0 \\ s(\alpha) + \epsilon ac(\alpha) & 0 & 0 \end{bmatrix} \quad (6)$$

and

$$[\hat{Q}_p] = \begin{bmatrix} 0 & -\epsilon c(\alpha) & -\epsilon s(\alpha) \\ \epsilon c(\alpha) & 0 & 0 \\ \epsilon s(\alpha) & 0 & 0 \end{bmatrix} \quad (7)$$

Equation (5) can be expanded and the higher-power terms neglected, resulting in a form which is computationally advantageous:

$$\hat{H}_2 \delta \theta_2 + \hat{H}_3 \delta \theta_3 + \hat{H}_4 \delta \theta_4 + \hat{H}_5 \delta \theta_5 + \hat{H}_6 \delta \theta_6 + \hat{H}_7 \delta D_6 = \hat{B}^T - \hat{I} \quad (8)$$

where

$$\hat{H}_i = (\hat{A}_i \hat{A}_2 \dots \hat{A}_{i-1}) \hat{Q}_x (\hat{A}_1 \hat{A}_2 \dots \hat{A}_{i-1})^T \quad (9)$$

and

$$\hat{A}_1 \hat{A}_2 \hat{A}_3 \hat{A}_4 \hat{A}_5 \hat{A}_6 = \hat{B} \quad (10)$$

Equation (10) can be written in a more compact form as

$$\hat{F} = \hat{B}^T - \hat{I} \quad (11)$$

Writing out each term of equation (11) produces two 3×3 dual-number matrices:

$$\begin{bmatrix} \hat{F}_{1,1} & \hat{F}_{1,2} & \hat{F}_{1,3} \\ \hat{F}_{2,1} & \hat{F}_{2,2} & \hat{F}_{2,3} \\ \hat{F}_{3,1} & \hat{F}_{3,2} & \hat{F}_{3,3} \end{bmatrix} = \begin{bmatrix} \hat{B}_{1,1} - \hat{I} & \hat{B}_{2,1} & \hat{B}_{3,1} \\ \hat{B}_{1,2} & \hat{B}_{2,2} - \hat{I} & \hat{B}_{3,2} \\ \hat{B}_{1,3} & \hat{B}_{2,3} & \hat{B}_{3,3} - \hat{I} \end{bmatrix} \quad (12)$$

This matrix equation comprises nine dual equations, only three of which are independent. Using the three terms in the upper-right triangle of each matrix and separating them into a set of real equations and a set of dual equations produces:

$$\begin{aligned} F_{\text{real},1,2} &= B_{\text{real},2,1} \\ F_{\text{real},1,3} &= B_{\text{real},3,1} \\ F_{\text{real},2,3} &= B_{\text{real},3,2} \end{aligned} \quad (13)$$

and

$$\begin{aligned} F_{\text{dual},1,2} &= B_{\text{dual},2,1} \\ F_{\text{dual},1,3} &= B_{\text{dual},3,1} \\ F_{\text{dual},2,3} &= B_{\text{dual},3,2} \end{aligned} \quad (14)$$

The real set, equation (13), however, does not include the constraint that the diagonal terms must each be equal to unity at closure. This constraint can be included either as three additional equations as described by Uicker, Denavit, and Hartenberg (1964) or through modification of the current equations set as discussed in Sandor and Erdman (1984). Adopting the second method modifies equation (13) to

$$\begin{aligned} F_{\text{real},1,2} &= B_{\text{real},2,1} + B_{\text{real},1,1} + B_{\text{real},2,2} - 2 \\ F_{\text{real},1,3} &= B_{\text{real},3,1} + B_{\text{real},1,1} + B_{\text{real},3,3} - 2 \\ F_{\text{real},2,3} &= B_{\text{real},3,2} + B_{\text{real},2,2} + B_{\text{real},3,3} - 2 \end{aligned} \quad (15)$$

The left-hand side of equations (14) and (15) contain the linear combination of the respective elements of the \hat{H} matrices and the error terms as can be seen from the left-hand side of equation (8).

Equations (14) and (15) can be combined as partitions of a single matrix of real-number equations. The resultant equation will have the form:

$$\begin{bmatrix} M_{\text{real}} \\ \dots \\ M_{\text{dual}} \end{bmatrix} \begin{bmatrix} \Delta \end{bmatrix} = \begin{bmatrix} V_{\text{real}} \\ \dots \\ V_{\text{dual}} \end{bmatrix} \quad (16)$$

where

$$M = \begin{bmatrix} H_{2r,1,2} & H_{3r,1,2} & H_{4r,1,2} & H_{5r,1,2} & H_{6r,1,2} & H_{7r,1,2} \\ H_{2r,1,3} & H_{3r,1,3} & H_{4r,1,3} & H_{5r,1,3} & H_{6r,1,3} & H_{7r,1,3} \\ H_{2r,2,3} & H_{3r,2,3} & H_{4r,2,3} & H_{5r,2,3} & H_{6r,2,3} & H_{7r,2,3} \\ \dots & \dots & \dots & \dots & \dots & \dots \\ H_{2d,1,2} & H_{3d,1,2} & H_{4d,1,2} & H_{5d,1,2} & H_{6d,1,2} & H_{7d,1,2} \\ H_{2d,1,3} & H_{3d,1,3} & H_{4d,1,3} & H_{5d,1,3} & H_{6d,1,3} & H_{7d,1,3} \\ H_{2d,2,3} & H_{3d,2,3} & H_{4d,2,3} & H_{5d,2,3} & H_{6d,2,3} & H_{7d,2,3} \end{bmatrix} \quad (17)$$

$$V = \begin{bmatrix} B_{\text{real}2,1} + B_{\text{real}1,1} + B_{\text{real}2,2} - 2 \\ B_{\text{real}3,1} + B_{\text{real}1,1} + B_{\text{real}3,3} - 2 \\ B_{\text{real}3,2} + B_{\text{real}2,2} + B_{\text{real}3,3} - 2 \\ \hline B_{\text{dual}2,1} \\ B_{\text{dual}3,1} \\ B_{\text{dual}3,2} \end{bmatrix} \quad (18)$$

and

$$\Delta = \begin{bmatrix} \delta\theta_2 \\ \delta\theta_3 \\ \delta\theta_4 \\ \delta\theta_5 \\ \delta\theta_6 \\ \delta D_6 \end{bmatrix} \quad (19)$$

Rearrangement of equation (16) to solve for the error terms produces the required equation for the Newton-Raphson iteration technique:

$$\Delta = M^{-1} V \quad (20)$$

The guesses of the displacement variables θ_n and D_n are revised by the error terms, Δ , and this new set of joint variable positions is used in the next iteration to compute a new set of error terms. Convergence is obtained when each of the error terms obtained from equation (20) is less than some specified resolution limit.

After obtaining a solution for the given position of the independent variable θ_1 , a new position is selected and the entire process repeated. The solution set from the previous position is used as the starting values for the new iteration. The step size between successive positions must be small enough to allow the Newton-Raphson technique to find closure. This step size depends upon the specified mechanism and varies

with its position. It is usually safe to use 20 degrees as a maximum step size.

Equations for the Davidon-Fletcher-Powell Optimization Method. If perfect guesses of the displacement variables are substituted into equation (10), then matrix B will be the identity matrix as required by equation (3), the condition of loop closure. For imperfect guesses, matrix B will differ from the identity matrix, implying lack of closure. The difference between matrix B and the identity matrix can be embodied in an objective function such as

$$F = \sum_{i=1}^3 \sum_{j=1}^3 [[B_{\text{real}}]_{ij} - [I]_{ij}]^2 + [B_{\text{dual}}]_{ij}^2 \quad (21)$$

which vanishes at closure but is greater than zero when closure does not occur. An optimization method can solve equation (3) by minimizing the objective function given by equation (21).

The DFP algorithm requires a set of gradients for each variable in addition to the objective function. The gradients provide the slope of the objective function with respect to each variable and are found by differentiation of equation (21) to be

$$G_i = 2 \sum_{j=1}^3 \sum_{k=1}^3 [[B_{\text{real}}]_{jk} - [I]_{jk}] \frac{\partial [B_{\text{real}}]_{jk}}{\partial x_i} + 2 \sum_{j=1}^3 \sum_{k=1}^3 [B_{\text{dual}}]_{jk} \frac{\partial [B_{\text{dual}}]_{jk}}{\partial x_i} \quad (22)$$

Equations (21) and (22) are used by the DFP method to find a solution. The DFP algorithm is described in detail by Fox (16) and basically consists of selecting the direction of steepest descent of the objective function from the variable vector, proceeding in that direction by an amount determined by the closeness of the objective function to the target value (in this case, zero) and then repeating three steps until the convergence criteria is satisfied.

Experimental Investigation

A series of experiments were conducted to validate the results of the numerical analysis. An experiment apparatus in-

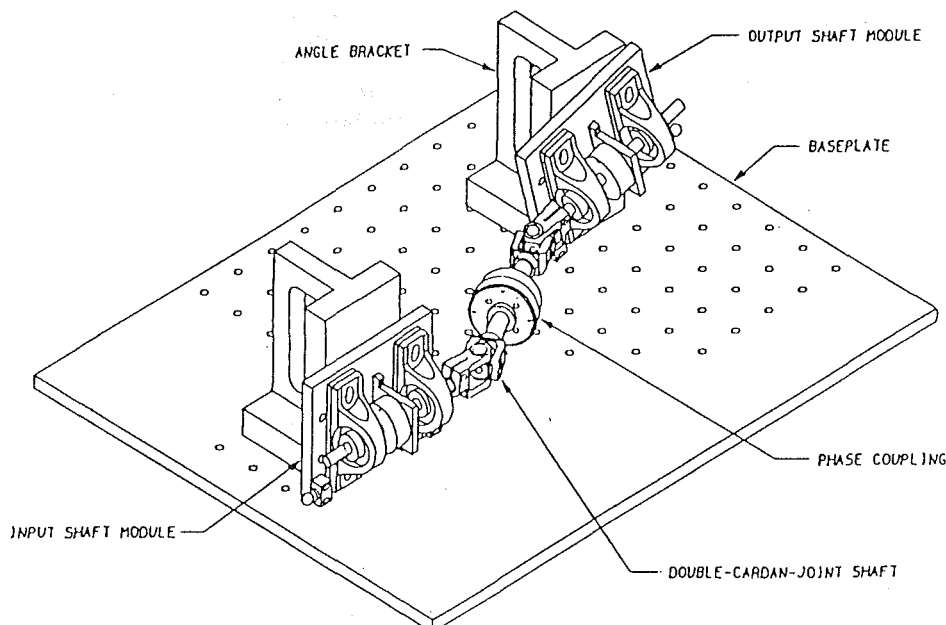


Fig. 3 Experimental apparatus

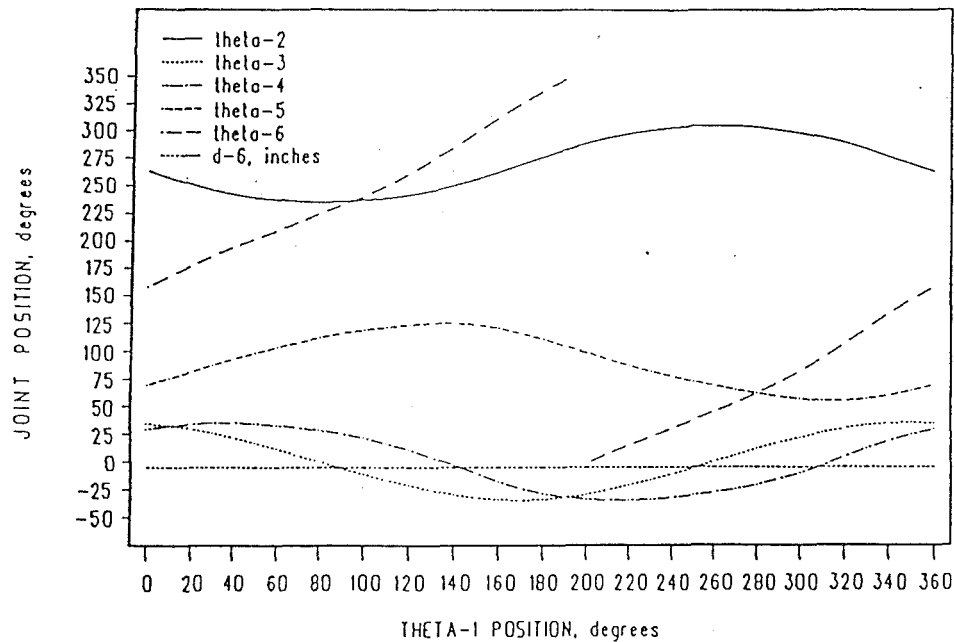


Fig. 4 Computed joint motions offset angles both 35 deg., offset 0.867 in., phase angle 50 deg.

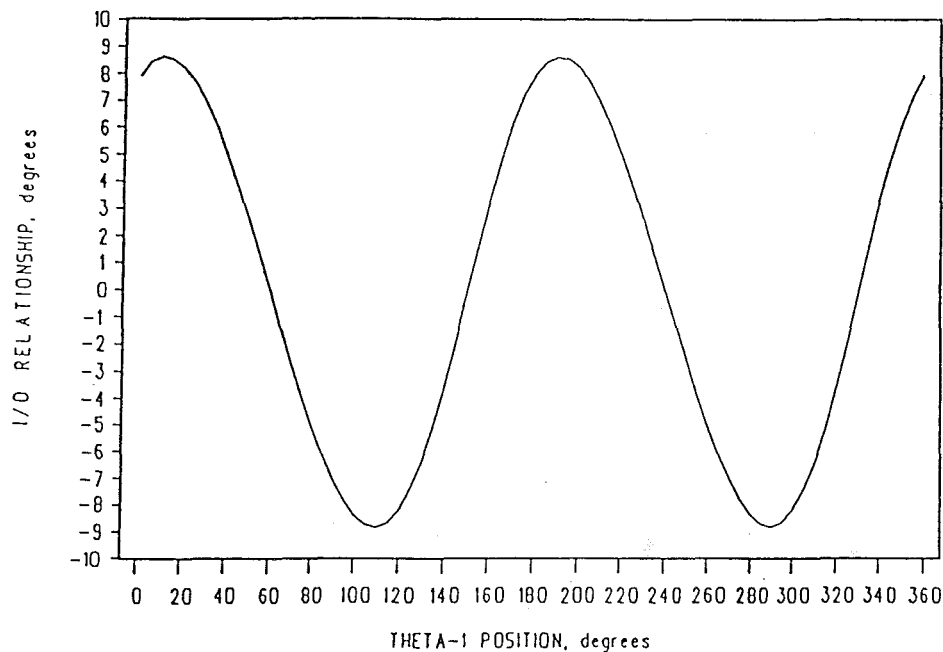


Fig. 5 Computed I/O relationship offset angles both 35 deg., offset 0.867 in., phase angle 50 deg.

corporating a double-Cardan-joint driveline was designed on a modular basis so that the offset angle at each Cardan joint, the angle between the input and output shafts, the offset distance between the input and output shafts and the phase angle between the two Cardan joints could be varied. It is illustrated in Fig. 3. Although provided for in the analysis, the experiment apparatus did not permit variation of link angular dimensions and joint-axis offsets within the two Cardan joints. Both the input and output shafts were equipped with optical shaft encoders to measure rotation. These were interfaced to a microcomputer for data acquisition.

Results and Conclusions

The numerical solution is capable of producing data on the

motion of each joint in the double-Cardan-joint driveline. A plot of the joint motions for a typical double-Cardan-joint driveline are shown in Fig. 4. R -type joints numbered 2 through 5 display single-cycle variation per revolution of the input shaft. Motion of prismatic joint D_6 is zero for this example. The motion of the output shaft is displayed as angle θ_6 and varies with two cycles per input-shaft revolution. This nonuniform motion can best be visualized by the input-output (IO) relationship, the lead and lag of the output-shaft rotation with respect to the input-shaft rotation. Figure 5 illustrates the IO relationship for the joint motions in Fig. 3.

If tolerance errors result in offset joint axes, then sliding will occur at the prismatic joint. Figure 6 shows the sliding which was computed by the numerical method for a double-

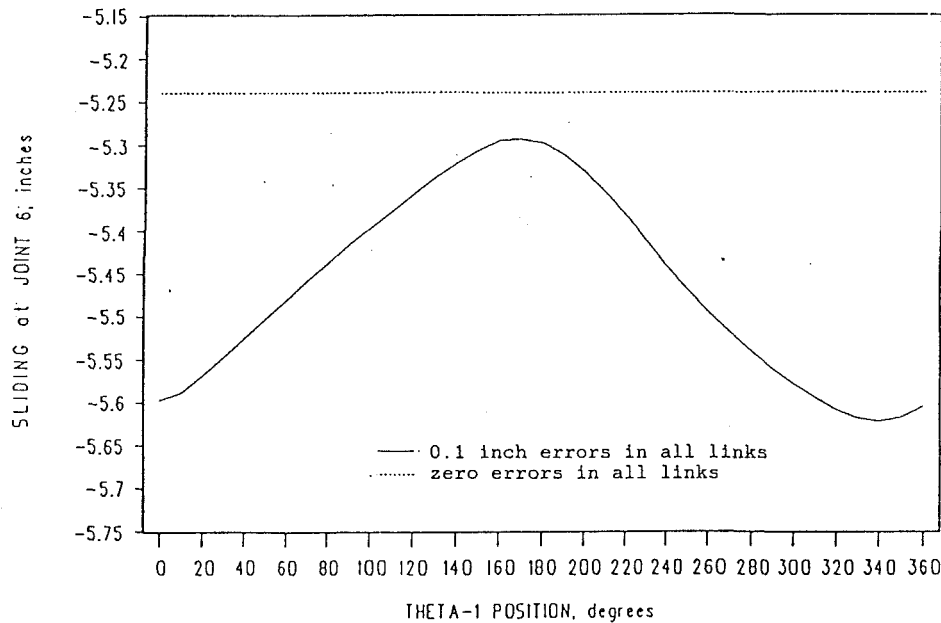


Fig. 6 Computed D_6 motion for a mechanism with dimensional errors in the links offset angles both 35 deg., offset 0.867 in., phase angle 50 deg.

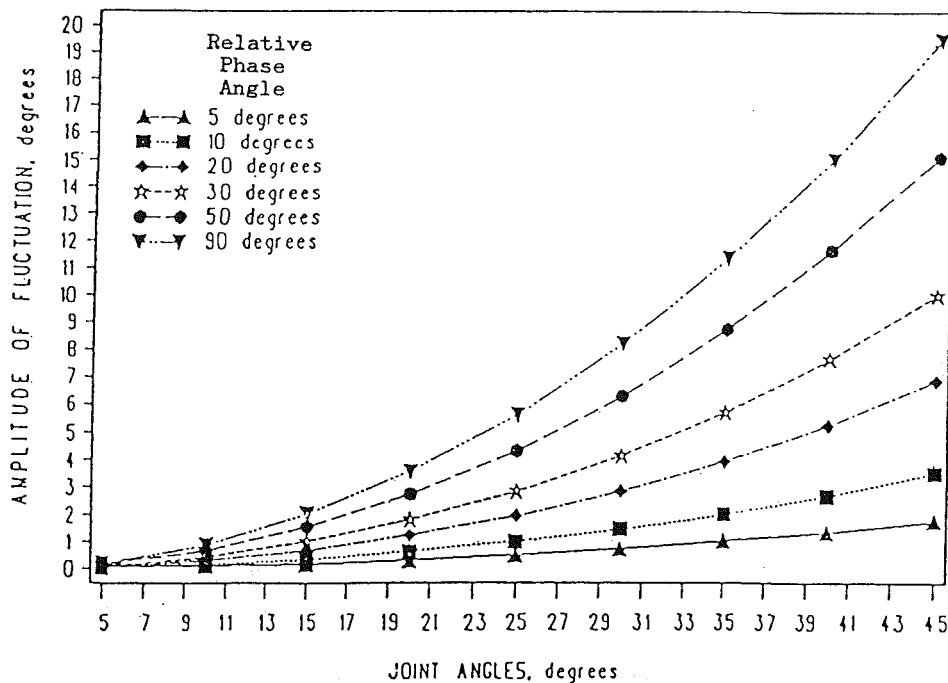


Fig. 7 Effect of relative phase angle on I/O displacement relationship

Cardan-joint driveline similar to that used to produce Fig. 5, but with joint-axis offsets of 0.1 inches. For comparison, the motion of the same driveline but with zero joint-axis-offset tolerance errors is also shown in Fig. 6.

Relative Phase Angle. If the input and output shafts do not intersect, but are offset by a certain distance, then the plane formed by the output and intermediate shafts and the plane formed by the input and intermediate shafts are displaced from one another by the "angle of twist." The relationship between the two planes each containing one of the Cardan-joint yokes which are mounted on the intermediate shaft (angle ϕ in Fig. 1) is called the "phase angle." The "relative phase angle," RPA, is defined as

$$\text{RPA} = (\text{phase angle}) - (\text{angle of twist}) \quad (23)$$

The importance of the relative phase angle is observed in Fig. 7. For a driveline with equal joint angles, the amplitude of fluctuation in output displacement increases significantly with relative phase angle to a maximum amplitude occurring at a relative phase angle of 90 degrees. In the figure it is observed that for joint angles of 45 degrees, about the largest experienced in practical applications, the fluctuation can range from zero degrees for RPA = 0 degrees to 20 degrees when RPA = 90 degrees.

Offset of Shaft Axes. As seen in Fig. 8, for a given RPA,

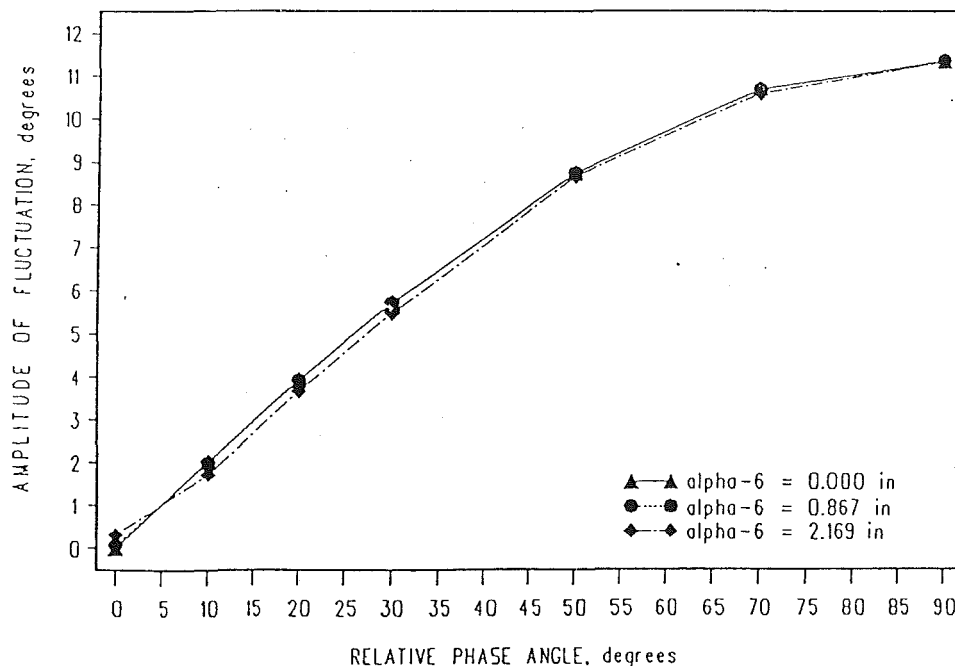


Fig. 8 Effect of offset on I/O relationship

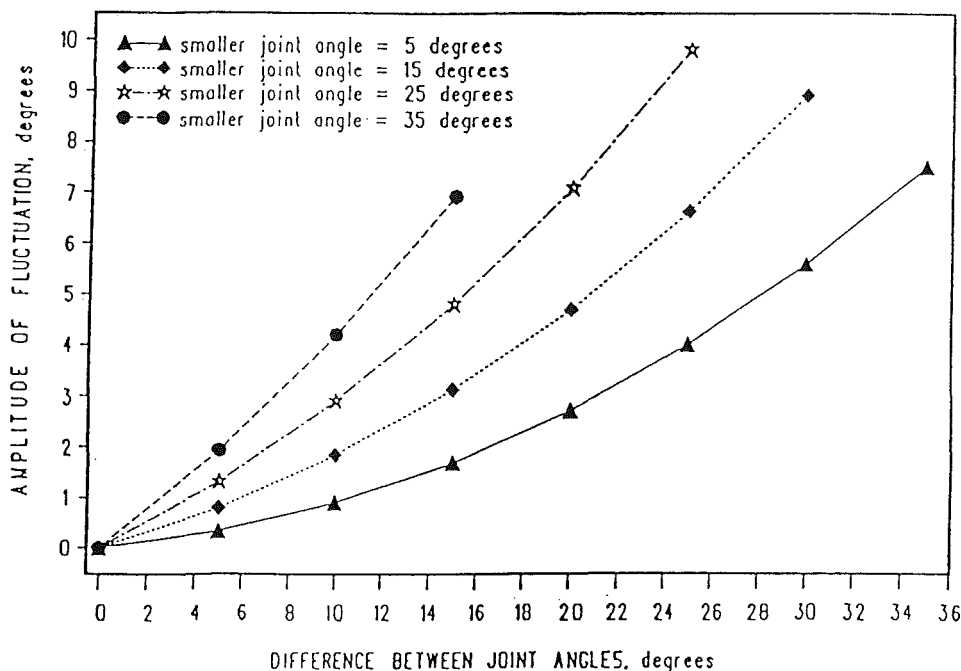


Fig. 9 Effect of unequal joint angles on I/O relationship

variation of the offset of the input and output shafts has negligible effect on the *IO* displacement relationship.

Unequal Joint Angles. When both joint angles in the driveline are equal, then arranging the mechanism so that the relative phase angle is zero will cause fluctuation in the input-output relationship to vanish. Thus for $RPA=0$, when the phase angle equals the angle of twist, the double-Cardan-joint driveline will function as a constant-velocity coupling. This agrees with the results reported by Wagner (1979).

However, it has been observed in this study that unequal joint angles results in a situation where the joints cannot be phased to arrange for constant-velocity motion. It is apparent that the amplitude of input-output fluctuation is minimized

for zero relative phase angle. This is seen in Fig. 9 which provides a measure of the input-output fluctuation amplitude for various combinations of joint angles at zero RPA. Larger amplitudes would be obtained for non-zero RPA's. Several characteristics can be observed in Fig. 8:

- (1) Increasing the difference between the two joint angles results in larger amplitudes.
- (2) Larger joint angles, with the difference between them held constant, produce greater amplitudes.

These facts point to the conclusion that the need to minimize joint angle difference becomes ever more important with larger joint angles.

Experimental Results. Experiments were conducted for a variety of arrangements. The results for several phase angles in a typical arrangement of the input and output shafts are shown in Fig. 10. The irregularities in the curves are observed to have a magnitude of 0.36 degrees, equal to the resolution of the encoders. To evaluate the error, the experiment for which the joint angles were 10 and 30 degrees, the phase angle 60 degrees and the input-output shafts offset 0.867 in. was repeated four times to arrive at a standard deviation in the measure output of 0.0323 degrees. In that the measured amplitude of the fluctuation was about 4 degrees, the error had a magnitude of less than 1 percent of the peak signal. The small magnitudes of these errors indicated that the quality of the measurements was good.

A comparison of experimental and computed results for a typical arrangement of input and output shafts with several phase angles is shown in Figs. 11 and 12. It is observed that there is close correlation between the experimental and analytical results.

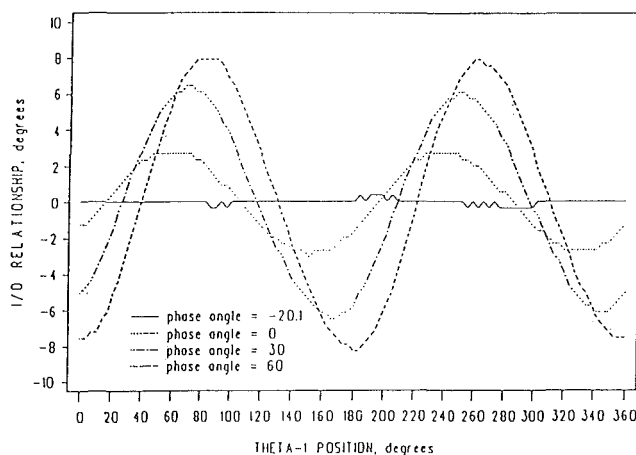


Fig. 10 Experimental measurement of I/O relationship offset angles both 30 deg., offset 0.867 in.

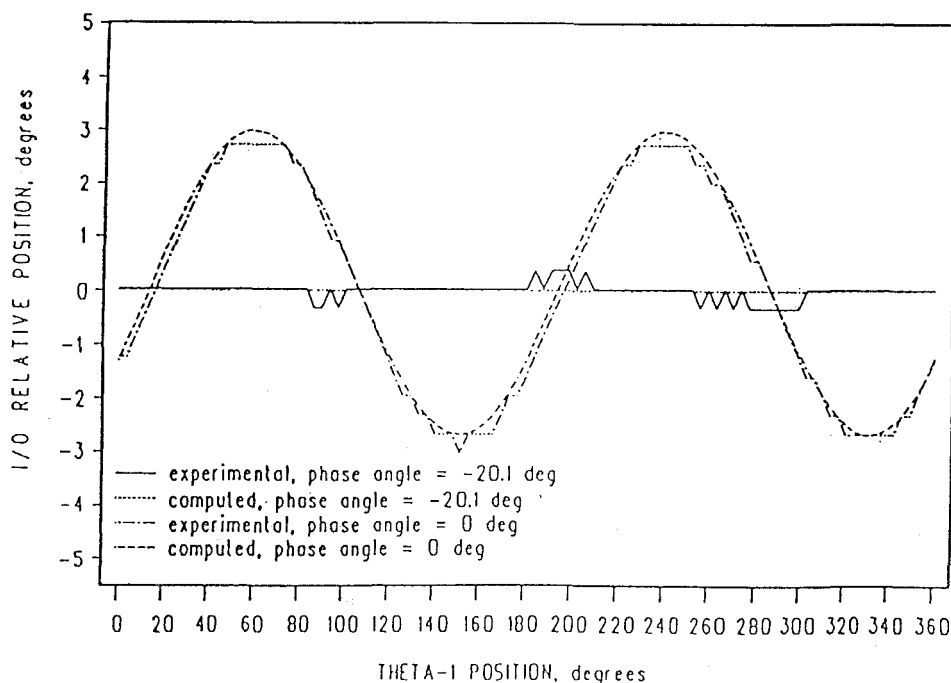


Fig. 11 Comparison of experimental and computed data phase angles 30 and 60 deg. Offset angles both 30 deg., offset 0.867 in.

Conclusions. The relative phase angle is the most important variable affecting the input-output displacement relationship of the double-Cardan-joint driveline. Relative phase angle is defined as the difference between the measured phase angle and the angle of twist between the planes of each Cardan joint. These planes are described geometrically by the center lines of the two shafts connected to either end of each Cardan joint.

Fluctuation in the input-output displacement relationship vanishes when the joint angles at the two Cardan joints are equal and the relative phase angle is set to zero.

Conditions where the two joint angles are unequal will always produce some fluctuation in the input-output displacement relationship no matter what the relative phase angle. The amplitude of this fluctuation is minimized when the relative phase angle is zero. If the difference between the joint angles and the relative phase angle are held constant, then the amplitude of fluctuation will increase for larger joint angles.

An estimate of the magnitude of these effects is obtained by noting that a double-Cardan-Joint driveline with both joint angles equal to 45 degrees has an input-output fluctuation amplitude that grows from zero to about 20 degrees as the relative phase angle is varied from zero to 90 degrees. The designer should remember the importance of the relative phase angle and the joint angle difference on the input-output displacement relationship, and that these quantities become increasingly more important with larger joint angles.

Acknowledgments

The authors appreciate the support of this research by the National Science Foundation through Grant No. MSM-8602189.

References

- Austin, T. C., Denavit, J., and Hartenberg, R. S., "Analysis of Errors in the Double Hooke Joint," *ASME JOURNAL OF ENGINEERING FOR INDUSTRY*, May 1965, pp. 251-257.
- Cooney, C. E., "Practical Procedures for Designing and Analyzing a Tandem Truck Driveline," SAE Paper 660413, 1966.
- Cowles, J. H., Jr., and Chiu, Y. P., "Computer-Aided Analysis of a Steering Column Using Cardan Universal Joints," SAE Technical Paper No. 841204, Passenger Car Meeting, Dearborn, MI, October 1-4, 1984.

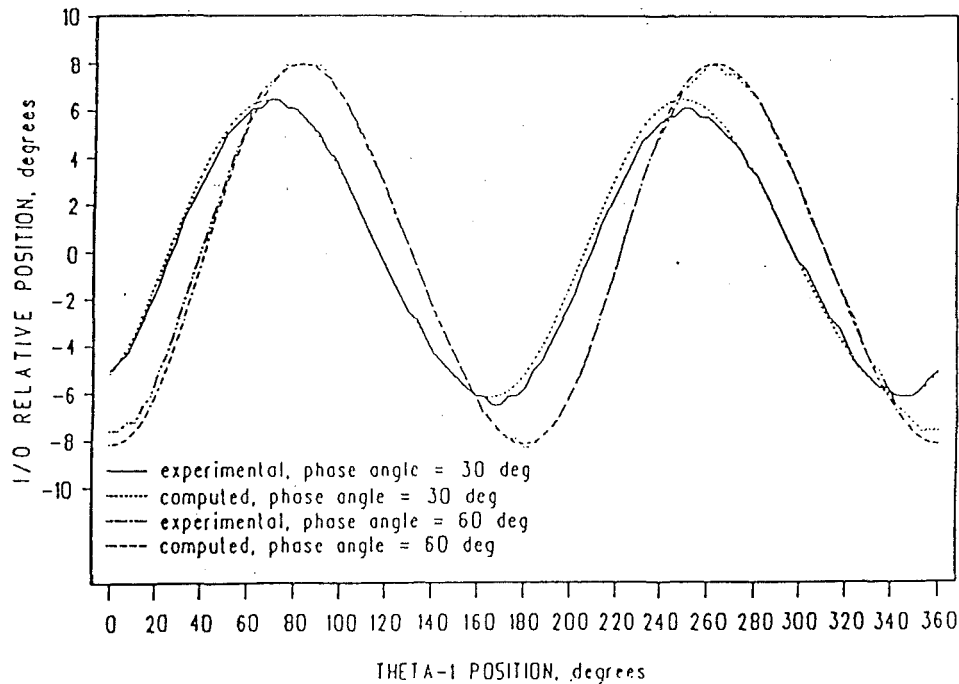


Fig. 12 Comparison of experimental and computed data phase angles -20.1 and 0 deg. Offset angles both 30 deg., offset 0.867 in.

Doughtie, V. L., and James, W. H., *Elements of Mechanism*, John Wiley & Sons, Inc., New York, NY, 1954.

Duffy, J., *Analysis of Mechanisms and Robot Manipulators*, Wiley-Interscience, Somerset, NJ, 1980.

Fischer, I. S., and Freudenstein, F., "Internal Force and Moment Transmission in a Cardan Joint with Manufacturing Tolerances," *ASME JOURNAL OF MECHANISMS, TRANSMISSIONS, AND AUTOMATION IN DESIGN*, Vol. 106, September 1984, pp. 391-311.

Fox, R. L., *Optimization Methods for Engineering Design*, Addison-Wesley Inc., Reading, MA, 1971.

Ju, X. L., and Duffy, J., "Displacement Analysis of Spatial Six-Link, 5R-C Mechanisms—A General Solution," *ASME JOURNAL OF MECHANISMS, TRANSMISSIONS, AND AUTOMATION IN DESIGN*, Vol. 107, September 1985, pp. 353-357.

Hall, A. S., Root, R. R., and Sandgren, E., "A Dependable Method for Solving Matrix Loop Equations for the General Three-Dimensional Mechanism," *ASME Journal of Engineering for Industry*, August 1977, pp. 547-550.

Mabie, H. H., and Ocvirk, F. W., *Mechanisms and Dynamics of Machinery*, John Wiley & Sons, Inc., New York, NY, 1975.

Maziotti, P. J., "Dynamic Characteristics of a Truck Driveline Systems," *SAE SP#262*, 1964.

Philipp, R. E., "Kinematics of a General Arrangement of Two Hooke's Joints," Technical Report 60-WA-37, ASME, November 1960.

Saari, O., "How to Obtain Useful Speed Variations With Universal Joints," *Machine Design*, October 1954, pp. 175-178.

Sandor, G. N., and Erdman, A. G., *Advanced Mechanism Design: Analysis and Synthesis*, Prentice Hall Inc., Englewood Cliffs, NJ, 1984, p. 621.

Tyson, H. N., *Kinematics*, John Wiley & Sons, Inc., New York, NY, 1954.

Uicker, J. J., Denavit, J., and Hartenberg, R. S., "An Iterative Method for the Displacement Analysis of Spatial Mechanisms," *ASME Journal of Applied Mechanics*, June 1964, pp. 309-314.

Wagner, E. R., "Useful Design Aids," *Universal Joint and Driveshaft Manual*, C. E. Cooney, ed., Society of Automotive Engineers, Warrendale, PA, 1979, pp. 411-415.